Articles

Proton NMR Assignments and Secondary Structure of the Snake Venom Protein Echistatin†

Yuan Chen,‡ Steven M. Pitzenberger,*,§ Victor M. Garsky,§ Patricia K. Lumma,§ Gautam Sanyal,∥ and Jean Baum*,‡

Chemistry Department, Rutgers University, Piscataway, New Jersey 08854, and Departments of Medicinal Chemistry and Pharmaceutical Research, Merck Sharp and Dohme Research Laboratories, West Point, Pennsylvania 19486

Received May 31, 1991; Revised Manuscript Received August 26, 1991

ABSTRACT: The snake venom protein echistatin is a potent inhibitor of platelet aggregation. The inhibitory properties of echistatin have been attributed to the Arg-Gly-Asp sequence at residues 24–26. In this paper, sequence-specific nuclear magnetic resonance assignments are presented for the proton resonances of echistatin in water. The single-chain protein contains 49 amino acids and 4 cystine bridges. All of the backbone amide, $C_\alpha H$, and side-chain resonances, except for the η-NH of the arginines, have been assigned. The secondary structure of the protein was characterized from the pattern of nuclear Overhauser enhancements, from the identification of slowly exchanging amide protons, from $^3J_{C\alpha H\text{-}NH}$ coupling constants, and from circular dichroism studies. The data suggest that the secondary structure consists of a type I β-turn, a short β-hairpin, and a short, irregular, antiparallel β-sheet and that the Arg-Gly-Asp sequence is in a flexible loop connecting two strands of the distorted antiparallel β-sheet.

Echistatin is one of several known snake venom proteins that inhibit the aggregation of activated platelets (Gan et al., 1988; Huang et al., 1987; Shebuski et al., 1989a; Dennis et al., 1990). Since platelet aggregation is a key step in thrombus formation, it is of interest to understand details of the inhibition on the molecular level. Knowledge of the structural requirements for platelet aggregation will ultimately be applicable to the discovery of medically useful antithrombotic agents.

Platelets adhere to one another and to vessel walls by forming noncovalent binding interactions between a cell surface receptor, called an integrin, and the Arg-Gly-Asp (RGD) sequence of extracellular matrix and adhesive proteins [for reviews see Ruoslahti and Pierschbacher (1986, 1987), Hynes (1987), and Ginsberg et al. (1988)]. The principal integrin on platelets is the glycoprotein IIb/IIIa complex (Phillips et al., 1988; Steiner et al., 1989). Adhesive proteins which bind to platelet Gp-IIb/IIIa[1] include fibrinogen, fibronectin, von Willebrand factor, and vitronectin. Because of its abundance, fibrinogen appears to be the most important of these proteins with respect to platelet aggregation in circulation (Plow et al., 1986). Several studies have shown that inhibition of fibrinogen binding to platelets with either antibodies (Gold et al., 1988; Yasuda et al., 1988; Coller et al., 1989) or Arg-Gly-Asp-based inhibitors (Shebuski et al., 1989a,b; Bush et al., 1989; McGoff et al., 1989) is an effective antithrombotic strategy.

Small synthetic peptides which contain the Arg-Gly-Asp sequence can duplicate the cell binding activity of the large extracellular proteins (Pierschbacher & Ruoslahti, 1984). Conformational studies have been reported on three peptides, H-Gly-Arg-Gly-Asp-Ser-Pro-OH in water (Reed et al., 1988; Mickos et al., 1990), Ac-Gly-Arg-Gly-Asp-Ser-Gly-NHEt in DMSO-d_6 (Genest et al., 1989; Nègre et al., 1989), and H-Arg-Gly-Asp-Ser-OH in water (Mickos et al., 1990). The studies indicate conformational preferences in a time-averaged sampling of conformational space. In one of our laboratories, we have studied the cyclic peptides Ac-Cys-Arg-Gly-Asp-Cys-OH and Ac-Cys-Arg-Gly-DAsp-Cys-OH in DMSO-d_6 and found them to exist as mixtures of conformers undergoing fast exchange on the NMR time scale (Bogusky et al., 1992). Although conformational preferences were found that could be related with biological activity, it is not known to what degree these solution conformations match the conformations of the peptides as they bind to the Gp-IIb/IIIa receptor. In order to better characterize the features of the Arg-Gly-Asp unit which are compatible with receptor binding, it is of interest to determine the structure of naturally occurring proteins which strongly bind to Gp-IIb/IIIa.

Echistatin is a 49 amino acid protein isolated from the saw-scaled viper *Echis carinatus*. It has roughly 2000-fold

† This research was supported by grants from Merck & Co. and the Searle Scholars Fund/Chicago Community Trust (J.B.).

* To whom correspondence should be addressed.

‡ Chemistry Department, Rutgers University.

§ Department of Medicinal Chemistry, Merck Sharp and Dohme Research Laboratories.

∥ Department of Pharmaceutical Research, Merck Sharp and Dohme Research Laboratories.

[1] Abbreviations: 2D, two dimensional; AMX, a spin system comprised of three nonequivalent spin $^1/_2$ nuclei—used here to generally describe amino acids with one C_α and two C_β protons; CD, circular dichroism; $d_{\alpha N}$, distance between the C_α proton of residue i and the amide NH proton of residue $i + 1$; $d_{\beta N}$, distance between the C_β proton of residue i and the amide NH proton of residue $i + 1$; d_{NN}, distance between the amide NH protons of sequential residues; DMSO, dimethyl sulfoxide; DQF-COSY, double-quantum-filtered correlation spectroscopy; FID, free induction decay; Gp-IIb/IIIa, glycoprotein IIb/IIIa complex, MLEV-16, isotropic mixing sequence, first described as a broad-band decoupling sequence by Levitt, Freeman, and Frenkiel (Levitt et al., 1982); NMR, nuclear magnetic resonance; NOE, nuclear Overhauser enhancement; NOESY, nuclear Overhauser effect spectroscopy; RELAY, single-relayed coherence transfer spectroscopy; TOCSY, total correlation spectroscopy; TPPI, time-proportional phase incrementation; TSP, sodium 3-(trimethylsilyl)propionate-d_4; U, Glu, Met, Lys, or Arg spin systems; UV, ultraviolet.

0006-2960/91/0430-11625$02.50/0

greater potency over the acyclic peptide Arg-Gly-Asp-Ser [inhibition of platelet aggregation; Gartner and Bennett (1985) versus Garsky et al. (1989)]. The Arg-Gly-Asp tripeptide unit is found at residues 24–26, and the protein contains eight cysteines. All of the cysteines except for Cys37 align with the sequences of the other known Arg-Gly-Asp-containing snake venom proteins (Dennis et al., 1990; Gould et al., 1990). Echistatin has been prepared synthetically by solid-phase synthesis and can be refolded to the biologically active conformation (Garsky et al., 1989).

In this paper we present sequence-specific assignments of the proton NMR spectrum of echistatin. All of the backbone amide and $C_\alpha H$ resonances and all of the side-chain resonances are assigned with the exception of the η-NH resonances of the arginines. Information about the secondary structure is obtained through the pattern of nuclear Overhauser enhancements (NOEs), values of vicinal J coupling constants along the backbone, and the relative hydrogen–deuterium exchange rates of the amide protons. The NMR data suggest that the Arg-Gly-Asp region of the protein is relatively unstructured; the tripeptide unit is found in a flexible loop anchored to a short segment of irregular antiparallel β-sheet.

Materials and Methods

Echistatin was prepared by solid-phase synthesis (Garsky et al., 1989).

Two types of samples were prepared for the NMR studies. In all cases, the concentration of echistatin ranged from 1.5 to 2.5 mM. In the first sample, lyophilized protein was dissolved in 90% H_2O/10% D_2O. Spectra of this sample exhibited all of the amide proton resonances. The second sample was prepared by dissolving the protein in D_2O. NMR spectra of this sample were recorded immediately after dissolution in order to observe slowly exchanging amide proton resonances. Further experiments were performed on the second sample after it was lyophilized and redissolved in D_2O (99.996 atom % D). Spectra of the resulting solution showed only the slowest exchanging amide protons. Low pH values were chosen for nearly all of the studies in order to reduce the rates of hydrogen exchange (Wüthrich, 1986) and disulfide exchange catalyzed by adventitious thiols [see, for example, Creighton (1984b)]. The acidity of each sample was determined by direct readings with a pH meter and glass electrode at 23 °C. Acidity values for the D_2O solutions are reported as pH* since no corrections were made for the deuterium isotope effect. Although pH* values may be converted to pD values with the equation pD = pH* + 0.4 (Glasoe & Long, 1960), there is a similar correction to pK_as for the deuterium isotope effect which is nearly equal to the isotope effect on a pH electrode (Bundi & Wüthrich, 1979). Thus, the ionization states of proteins in H_2O and D_2O are similar when the pH for an H_2O solution is roughly the same as the pH* (not pD) of a D_2O solution. pH and pH* adjustments were made by adding small quantities of 0.1 M NaOD or 0.1 M DCl as needed. For the H_2O sample, experiments were run at different pHs (3.1, 3.5, and 4.2) in order to eliminate ambiguities in the assignment. Experiments were run at pH* values of 3.1, 4.4, 5.7, and 7.1 for the sample in D_2O. Reported chemical shifts are referenced to internal TSP (30 μM).

All NMR experiments were run at 27 °C on a Varian VXR-500S spectrometer at 500 MHz. Double-quantum-filtered correlation spectroscopy (DQF-COSY) (Bax & Freeman, 1981; Nagayama et al., 1980; Rance et al., 1983; Shaka & Freeman, 1983), total correlation spectroscopy (TOCSY) (Braunsweiler & Ernst, 1983) with a mixing time of 55 ms, single-relayed coherence transfer spectroscopy (RELAY) (Eich et al., 1982) with relay times of 18, 20, and 25 ms, and nuclear Overhauser effect experiments (NOESY) (Kumar et al., 1980; Otting et al., 1986) with mixing times of 50, 100, 150, 175, 200, 300, and 350 ms were recorded. A "pretocsy" pulse sequence with an isotropic mixing time of 20 ms was integrated into the RELAY and NOESY experiments for the samples in H_2O in order to recover α-proton resonances that would otherwise be bleached by preirradiation of the H_2O resonance (Otting & Wüthrich, 1987). Isotropic mixing in the TOCSY and pretocsy experiments was achieved by the MLEV-16 pulse sequence (Braunsweiler & Ernst, 1983; Bax & Davis, 1985). To achieve sign discrimination in the t_1 dimension, 2D spectra were recorded by the hypercomplex method (Mueller & Ernst, 1979; States et al., 1982). For certain experiments, the time-proportional phase incrementation (TPPI) method (Redfield & Kunz, 1975; Marion & Wüthrich, 1983) was used in place of the hypercomplex method in order to minimize the water frequency artifact in the ω_1 dimension. Quadrature detection was used in the t_2 dimension for all experiments.

NOESY and TOCSY data sets consisted of 2048 data points in the t_2 dimension and either 256 (hypercomplex method experiments) or 512 (TPPI method experiments) t_1 increments. For DQF-COSY and RELAY experiments, 2048 data points were acquired in the t_2 dimension with either 512 (hypercomplex method) or 1024 (TPPI method) t_1 increments. FIDs were multiplied by skewed phase-shifted sine bell window functions prior to complex Fourier transformation. Data were zero-filled to 2048 real points in both dimensions, resulting in a digital resolution of 2.7 Hz/point. Fourier transformation was carried out on an Iris workstation using FTNMR software (Hare Research, Inc.).

Vicinal $^3J_{C\alpha H\text{-}NH}$ coupling constants were obtained from DQF-COSY experiments acquired with either 4096 or 8192 data points in the t_2 dimension. FIDs were zero-filled to 4096 or 16 384 real data points in the t_2 dimension prior to Fourier transformation, resulting in a digital resolution of 1.3 and 0.4 Hz/point, respectively. Data were processed using a 1.5-Hz Lorentzian window function in the t_2 dimension and either a 90° phase-shifted sine bell or a Gaussian function in the t_1 dimension. Line width independent $^3J_{C\alpha H\text{-}NH}$ coupling constants were calculated from the data by the method of Kim and Prestegard (1989). Vicinal $^3J_{C\alpha H\text{-}NH}$ coupling constants were also obtained from 1D spectra of echistatin which exhibited resolved or nearly resolved resonances because of partial exchange, chemical shift, or narrow line width. The 1D couplings were measured by peak deconvolution using the standard fitting procedure found in VNMR software (Varian Instruments).

Circular dichroism (CD) measurements were made using a Jasco J-720 CD spectrometer. A quartz cuvette of 1-mm path length, containing the sample, was placed in a thermostated cell holder which was maintained at 26 °C. Echistatin solutions were prepared by dissolving lyophilized protein in 5 mM sodium phosphate buffer at final pH values of 3.4 and 7.3. The concentration of echistatin in these solutions was determined from ultraviolet (UV) absorption spectra using a molar extinction coefficient of 1780 M^{-1} cm^{-1} at 280 nm, calculated for contributions from a single tyrosine residue and four disulfide bridges (Cantor & Schimmel, 1980). Echistatin concentrations ranged from 35 to 45 μM. Far-UV CD spectra in the wavelength range of 184–260 nm were analyzed for secondary structure by the variable selection method of Johnson and co-workers, which is based on the singular value decomposition theory (Manavalan & Johnson, 1987). The

fractional contributions of different secondary structures were estimated by an unconstrained analysis, followed by selection of fits that yielded values between 0.9 and 1.1 for the sum of fractions and less than 0.2 for root mean squared errors.

Results and Discussion

Sequential assignments were achieved via the established procedure of first classifying the residues by type, second establishing connectivities between neighboring residues by proton–proton NOEs, and then identifying short segments of residues and matching these segments to the protein sequence (Wüthrich, 1986). Because of significant overlap in the $C_\alpha H$ and amide proton regions, it was necessary to classify as many amino acid spin systems as possible before beginning the sequential assignments. The spin systems were thus divided into 12 groups. It was also necessary to acquire spectra at different pHs in order to eliminate ambiguities which otherwise arise in the sequential assignments.

Amino Acid Spin System Identification. Analysis of the amino acid spin systems began with the amide to aliphatic proton region of the TOCSY spectrum of echistatin dissolved in H_2O (Figure 1). The C_α proton resonances were identified by comparison with the fingerprint region of the DQF-COSY spectrum (H_2O). Most of the C_β proton resonances in the TOCSY spectrum were recognized by comparison with the RELAY spectrum. Four groups of spin systems were initially identified from the TOCSY experiment by inspection of the NH to $C_\alpha H$, $C_\beta H$, $C_\gamma H$, and $C_\delta H$ connections. The four groups were (1) Gly with two C_α proton resonances, (2) Thr and Ala spin systems, (3) AMX spin systems with C_β proton resonances between 2.5 and 4.0 ppm, and (4) long side chain spin systems (Lys, Glu, Arg, etc.) where at least three cross peaks from the side chain to the amide proton were observed. The tentative classification of these amino acid spin systems was confirmed by analyzing the cross peaks between the side-chain protons in DQF-COSY, RELAY, and TOCSY spectra of the protein in D_2O.

Five Gly and seven methyl-containing residues (two Ala, three Thr, one Leu, and one Ile) were unambiguously assigned. Four Gly residues with different $C_\alpha H$ resonances were identified by observing pairs of $C_\alpha H$ to NH cross peaks in the fingerprint region of the DQF-COSY spectrum of echistatin in H_2O (Figure 1B) and by the characteristically large J couplings between the C_α proton pairs. The fifth Gly residue, which has degenerate $C_\alpha H$ chemical shifts, was identified later during the sequential analysis. The amide proton of the fifth glycine is slowly exchanging and is resolved as a triplet in the one-dimensional spectrum, thereby confirming the sequential assignment. Two out of the three Thr residues have different C_α and C_β proton chemical shifts and were identified unambiguously from the RELAY spectrum via $C_\alpha H$ to $C\gamma H$ cross peaks. In addition, the amide to C_α, C_β, and C_γ proton cross peaks were observed in the RELAY and TOCSY spectra. The third Thr has degenerate C_α and C_β proton chemical shifts. A strong COSY cross peak was observed in the same region as the Ala $C_\alpha H$ to $C_\beta H$ cross peaks and the Thr $C_\beta H$ and $C_\gamma H$ cross peaks, and an amide to C_γ proton cross peak was observed in the TOCSY spectrum (H_2O) for this third Thr residue. In addition, a "forbidden" amide to C_γ proton cross peak, due to the strong coupling between C_α and C_β protons (Kay et al., 1987), was observed in the RELAY spectrum. The two Ala residues were assigned by observing the strong COSY cross peaks between C_α and C_β protons and RELAY peaks between amide and C_β protons. The single Ile and Leu spin systems were unambiguously identified. The nearly degenerate $C_\beta H$ and one of the C_γ protons of the Ile were resolved in the course of a pH titration experiment. For both spin systems, the complete pattern of scalar coupling connectivity between protons on the side chains was observed.

Figure 2A, an expansion of a DQF-COSY spectrum (D_2O), shows $C_\alpha H$ to $C_\beta H$ cross peaks of 20 AMX spin systems. Echistatin contains three Asn, one Phe, one Tyr, one His, one Ser, eight Cys, and five Asp residues. The three Asn residues were distinguished from other AMX spin systems through an NOE cross peak between the C_β and the δ-NH_2 protons of each Asn in the NOESY spectrum of the protein in H_2O. The aromatic ring protons of Phe, Tyr, and His were readily determined by inspection of the spectra. The AMX spin systems of these aromatic residues were assigned on the basis of NOEs between the aromatic protons and the respective C_β protons of the residues (Wagner & Wüthrich, 1982; Wider et al., 1982). The 14 remaining AMX spin systems consisting of one Ser, eight Cys, and five Asp residues were not distinguished from one another and were grouped together for sequential assignment purposes.

The $C_\alpha H$ to $C_\beta H$ cross peaks of the long side chain residues are shown in an expansion of the DQF-COSY spectrum (Figure 2B) of the protein in D_2O. Echistatin contains four Pro, four Arg, five Lys, one Met, and three Glu residues, in addition to the Leu and Ile residues discussed above. Of these spin systems, the four prolines were identified by observing the complete connectivity pattern between the protons. Since Arg and Lys residues occasionally have J coupling patterns similar to that of Pro, the Pro residues were distinguished by the absence of cross peaks due to the amide protons and side-chain NH protons. The proline residues were also distinguished by characteristic shifts of the C_β and C_γ proton resonances ($\sim$2.0–2.3 for Pro and $\sim$1.4–1.9 for Lys and Arg). The differentiation of Arg and Lys spin systems from Pro was confirmed by the sequential assignments. The Lys, Arg, Met, and Glu residues were not distinguished from each other and were placed in the same group.

At this stage, the 49 amino acids in the sequence were placed into 12 groups: (1) Asn; (2) Phe; (3) Tyr; (4) His; (5) other AMX spin systems; (6) Thr; (7) Ala; (8) Gly; (9) Leu; (10) Ile; (11) Pro; and (12) U, symbolizing Glu, Met, Lys, and Arg spin systems.

Sequential Assignments. Sequential assignments were undertaken by looking for $d_{\alpha N}$, d_{NN}, and $d_{\beta N}$ connectivities. The pretocsy–NOESY experiment (H_2O) with a 200-ms mixing time was used to obtain the $d_{\alpha N}$, d_{NN}, and $d_{\beta N}$ connectivities. For all but four dipeptide pairs, when a $d_{\alpha N}$-type NOE was observed, a sequential connectivity was established only if an additional $d_{\beta N}$ or d_{NN} NOE was also observed. With one exception, if no $d_{\alpha N}$ NOE was observed, then simultaneous observation of d_{NN} and $d_{\beta N}$ NOEs established sequential relationships (Billeter et al., 1982). Sequence assignments through prolines were determined by looking for sequential $d_{\alpha\delta}$ NOEs in a 200-ms NOESY experiment (D_2O). Resonance overlap was clarified by comparing spectra at different pHs.

Analysis of sequence segments used the classified amino acid spin systems (see above) and, in some instances, unambiguously assigned amino acids, Phe13, Leu14, Ile19, Tyr31, and His44. Initially, the following peptide segments were obtained through sequential NOE connections: U-AMX-Gly-Pro, U-Phe13-Leu14-U-U-Gly-Thr-Ile-AMX, AMX-AMX-Tyr31-AMX, U-Thr-AMX, AMX-Pro-U-Asn-Pro, and His44-U-Gly-Pro. These peptide fragments were assigned to residues 3–6, 12–20, 29–32, 35–37, 39–43, and 44–47, respectively, by comparison with the protein sequence. The remaining residues were assigned by extending the peptide

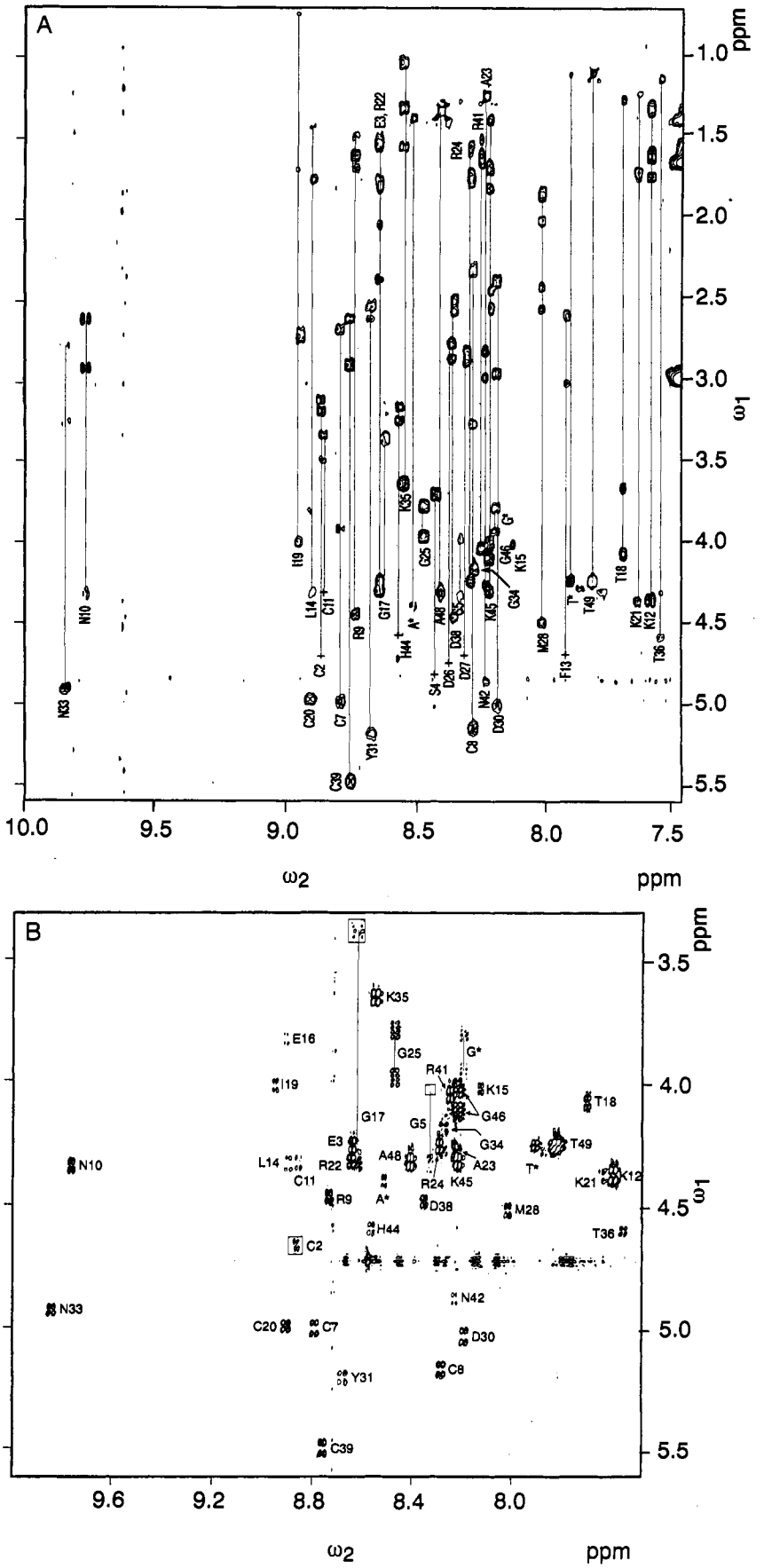

FIGURE 1: (A) NH–aliphatic region of the TOCSY spectrum of echistatin dissolved in 90% H_2O/10% D_2O at pH = 3.1 and 27 °C. Relayed connectivities are indicated by continuous lines. "+" indicates $C_\alpha H$ to amide NH cross peaks that were bleached by irradiation of the water resonance. Extra Thr, Ala, and Gly correlations are indicated with asterisks (see text). (B) The fingerprint region of the DQF-COSY spectrum of echistatin dissolved in 90% H_2O/10% D_2O at pH = 3.1 and 27 °C. A few $C_\alpha H$ to amide NH cross peaks are missing due to presaturation of the water resonance (the missing correlations were observed in spectra taken with the pretocsy pulse scheme). Extra Thr, Ala, and Gly correlations are indicated with asterisks. Boxed cross peaks were taken from a lower threshold spectrum.

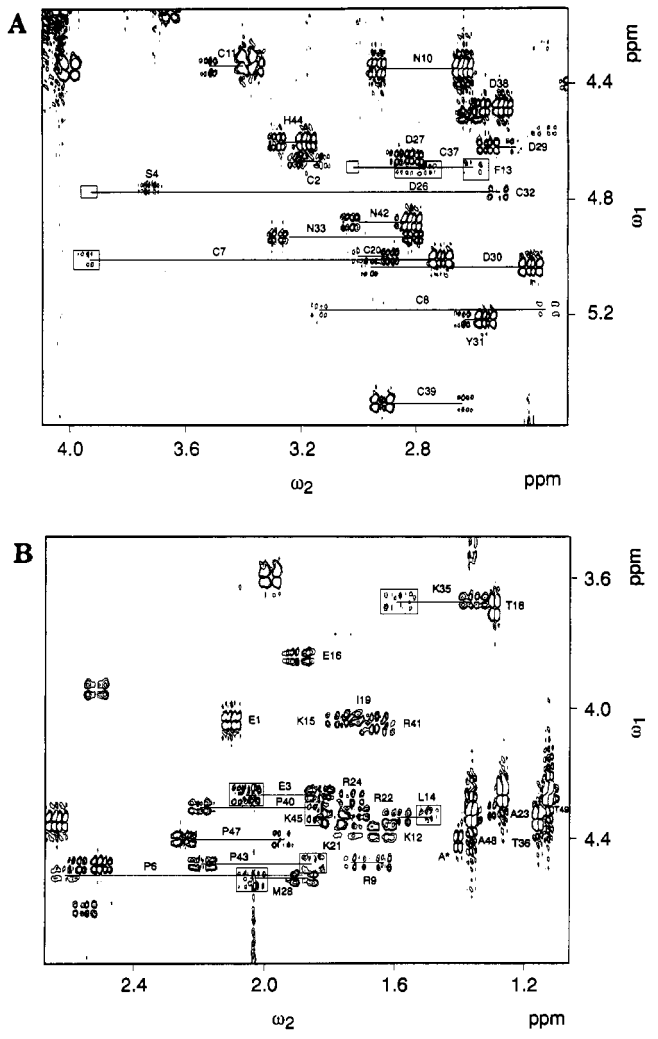

FIGURE 2: (A) Expansion of a DQF-COSY spectrum of echistatin dissolved in D_2O at pH = 3.1 and 27 °C showing 20 AMX spin systems. Cross peaks that are boxed were taken from a lower threshold spectrum. (B) Expansion of a DQF-COSY spectrum of echistatin dissolved in D_2O (pH = 3.1, 27 °C) showing the assignments of the C_α–C_β proton cross peaks of residues other than AMX spin systems. Boxed regions were taken from a spectrum plotted with a lower threshold.

segments via sequential connectivities. Figures 3 and 4, which are expansions of the pretocsy–NOESY spectrum (H_2O), illustrate the sequential $d_{\alpha N}$ and d_{NN} connections, respectively. Starting from the N-terminal end, Figure 3A shows the $d_{\alpha N}$ connections from Glu1 to Arg22. The sequential $d_{\alpha N}$ NOE cross peaks from Pro6 to Cys7 and Cys7 to Cys8 were weak but were observed at lower threshold levels in the NOESY spectrum (D_2O). At pH 3.5, the NOE cross peak of the amide to C_α proton of Arg9 overlaps with the $d_{\alpha N}$ NOE cross peak of Asp38 to Cys39. The two cross peaks were resolved and could be distinguished at pH 3.1. The sequential connectivities for residues Asn10, Cys11, and Lys12 were determined by d_{NN} NOEs (Figure 4) and $d_{\beta N}$ NOEs. In H_2O, the $d_{\alpha N}$ NOE between Gly17 and Thr18 is weak; however, it is confirmed in the D_2O NOESY spectrum where both Gly17 C_α protons show an NOE to the amide proton of Thr18. The sequential $d_{\alpha N}$ connectivities from Arg22 to Thr49 are shown in Figure 3B. The $d_{\alpha N}$ connection from Met28 to Asp29, which overlaps with the $d_{\alpha N}$ NOE cross peak between His44 and Lys45, was resolved at pH 3.1. The COSY cross peak of the $C_\alpha H$ to amide proton of Asp29 overlaps with the $d_{\alpha N}$ NOE cross peak from Asp29 to Asp30. These overlapping resonances were separated at pH 4.2. The d_{NN} NOE connections from Asn33 to Thr36 and from Cys37 to Asp38 are shown in Figure 4. The COSY cross peak of Lys45 in the fingerprint region overlaps with the $d_{\alpha N}$ cross peak from Lys45 to Gly46 at pH 3.1 and pH 3.5, but was resolved at pH 4.2. $d_{\alpha\delta}$ NOE connections were observed in a NOESY experiment (D_2O) for Gly5-Pro6, Cys39-Pro40, Asn42-Pro43, and Gly46-Pro47. These results indicate that the peptide bonds in each of these dipeptides are trans rather than cis (Wüthrich et al., 1984).

All the dipeptides that have sequential $d_{\alpha N}$ connectivities also have either $d_{\beta N}$ or d_{NN} connections, except for four cases. Sequential $d_{\beta N}$ or d_{NN} connections were not observed for Thr18-Ile19, Asp29-Asp30, Cys32-Asn33, and Ala48-Thr49. A $d_{\delta N}$ connectivity was observed for Thr18-Ile19. $d_{\beta N}$ or d_{NN} connections were not confirmed for Asp29-Asp30 because the amide proton chemical shifts are close at the three pH values studied. With the exception of Cys11-Cys12, the dipeptides which are missing $d_{\alpha N}$ connectivities have d_{NN} and $d_{\beta N}$ connectivities. The $d_{\alpha N}$ connectivity for Cys11 and Lys12 was not confirmed because the C_α proton chemical shifts are very close at all three pH values. Asp residues were independently confirmed by noting the upfield shifts of the C_β proton resonances with increasing pH. Similarly, the C_γ proton chemical shift of Glu3 was also found to be pH dependent (Bundi & Wüthrich, 1979). A summary of the NOE connectivities is presented in Figure 5, and chemical shifts for all the residues are listed in Table I. Instances of methylenes having degenerate chemical shifts in Table I are assumed when no other peak correlations could be found. Therefore, these assigned degeneracies should be considered tentative.

Values for 28 $C_\alpha H$–NH vicinal couplings are given in Figure 5. These were measured by the Kim and Prestegard method from 2D spectra (Kim & Prestegard, 1989) and by peak deconvolution of 1D spectra. Ten couplings were measured from the DQF-COSY spectrum of a freshly dissolved sample of the protein in D_2O. Nine additional couplings were measured in the DQF-COSY spectrum of the sample in H_2O. In the H_2O spectrum, coupling constants were not obtained for 8 of the C_α protons because of proximity to the water resonance, 25 of the C_α protons which have S/N ratios less than 10, 1 C_α proton which has degenerate α,β protons, and 1 C_α proton which is overlapped. For each of the 19 values derived from 2D spectra and reported in Figure 5, the S/N ratio is greater than 10, satisfying the minimal requirement for obtaining accurate values of J (Kim & Prestegard, 1989). Additional backbone coupling constants (total of 21; 10 redundant with those determined by the 2D method and 11 new ones) were obtained by applying peak deconvolution to 1D spectra of amide resonances. Fifteen couplings were determined from 1D spectrum of a freshly prepared D_2O solution of the protein where solvent exchange reduced the number of peaks in the amide region. Five backbone couplings were obtained from amide resonances which are resolved by chemical shift or by virtue of their relatively narrow line width in a 1D H_2O spectrum of the protein. Although an 8.3-Hz value was determined for Thr49, this value is not included in Figure 5 because the residue has degenerate $C_\alpha H$ and $C_\beta H$ chemical shifts.

A few cross peaks are present in the fingerprint region spectrum (see, for example, Figure 1B; marked with asterisks) which are weak and are in addition to the 49 assigned residues. These peaks were identified from DQF-COSY, TOCSY, and RELAY experiments as one Gly, one Ala, one Pro and one Thr. No NOE cross peaks involving these residues have been observed. It is possible that the extra cross peaks are from a minor conformation resolved on the NMR time scale, or they

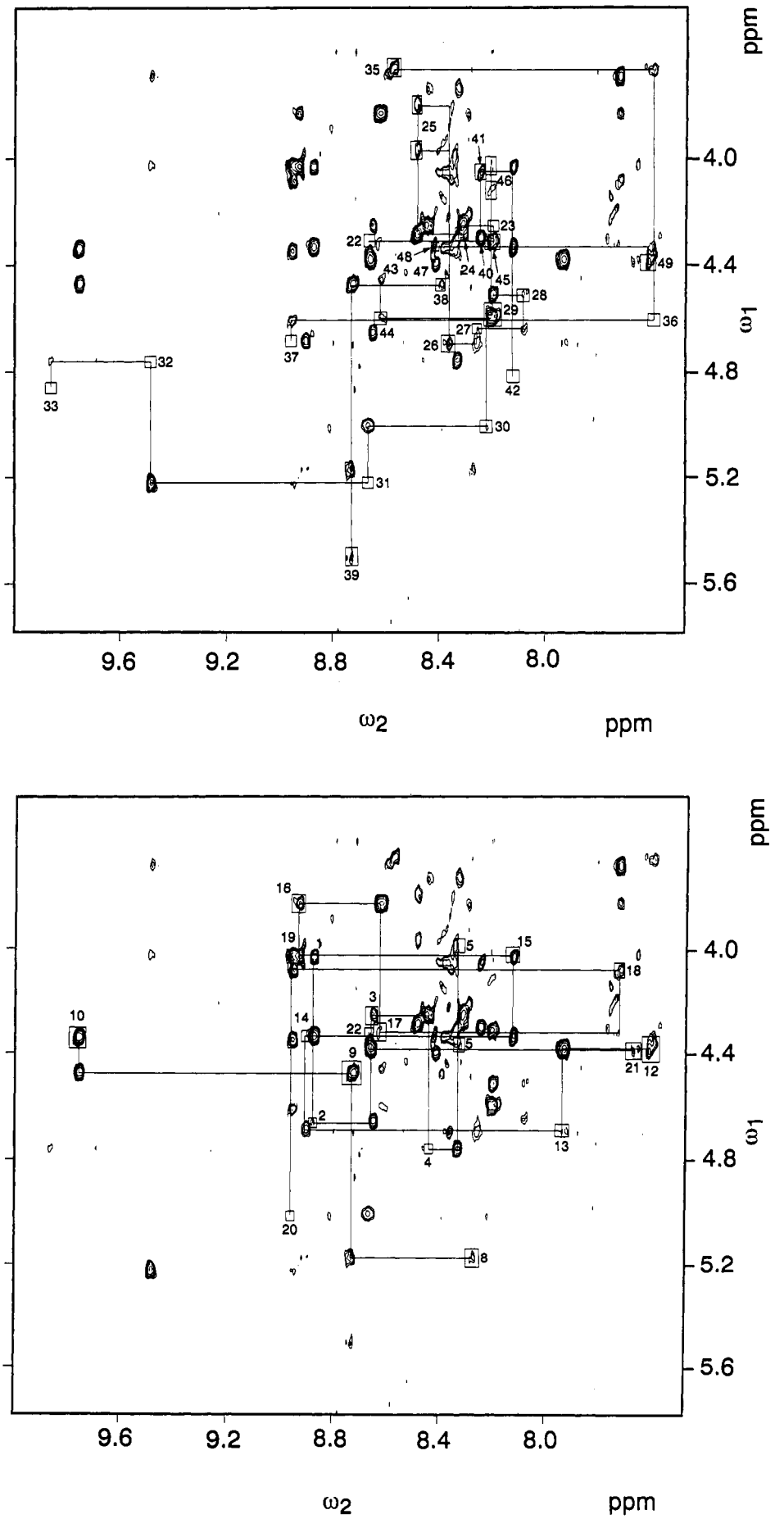

FIGURE 3: NOESY spectrum of echistatin dissolved in 90% H_2O/10% D_2O (pH = 3.1, 27 °C) showing sequential $d_{\alpha N}$ connectivities of (A) Glu 1 to Arg22 and (B) Ala23 to Thr49. The boxes represent the positions of the COSY cross peaks.

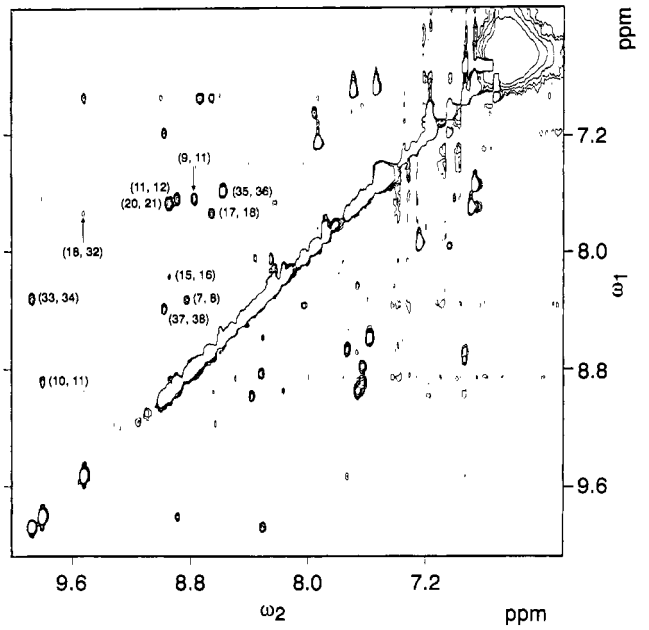

FIGURE 4: NOESY spectrum of echistatin dissolved in 90% H_2O/10% D_2O (pH = 3.1, 27 °C) with a mixing time of 175 ms showing the d_{NN} connectivities.

may arise from chemical decomposition of the protein as HPLC results showed extra components with time. Great care was taken in the sequential assignment of these residue types, and sequential assignments were never started from these spin systems.

Circular Dichroism Studies. CD spectra of echistatin were measured at pH 3.4 and 7.3 in 5 mM sodium phosphate buffer. The spectra are shown in Figure 6. The spectra are characterized by a minimum at 188–189 nm, a broad shoulder with negative ellipticity around 204 nm, and a weak maximum at approximately 225 nm. The variable selection method (see Materials and Methods) gave nearly identical estimates of secondary structure for both pH values. The estimated contributions of α-helix, β-pleated sheets, β-turns, and undefined structures are 2–8%, 24–36%, 27–33%, and 28–34%, respectively.

Because echistatin has four disulfide bonds among 49 residues, it was of concern to determine the magnitude of this contribution to the CD spectrum. Unfortunately, there is no satisfactory way of resolving S–S bond ellipticity from the peptide backbone CD signal because the chirality, orientation, and electrostatic interactions of S–S bonds in polypeptides are often undetermined factors and are therefore difficult to reproduce with model compounds. An attempted correction for the disulfide contribution, based on measurements of the L-cystine CD spectrum, did not significantly alter the secondary structure estimates presented above.

NMR pH Study. Acidic conditions (pH 3–4) were chosen for the secondary structure determination in order to minimize any possible complications from disulfide exchange and to facilitate the NMR expriments. The rate of thiol-catalyzed disulfide exchange is reduced under mildly acidic conditions [see, for example, Creighton (1984b)]. Also, amide hydrogen exchange with solvent is sufficiently slow at pH 3–4 to allow presaturation of water in NMR experiments without greatly affecting amide resonance intensities (Wüthrich, 1986). A concern over performing the structure determination at a nonphysiological pH was addressed in part by the CD studies described above. We cross-checked the CD result of minimal perturbation of structure between neutral and acidic environments by comparing α-proton chemical shifts in NMR spectra of echistatin at neutral and acidic pHs.

1D and DQF-COSY spectra were recorded in D_2O at pH* values of 3.1, 4.4, 5.7, and 7.1. Expected shifts were observed for protons near the titratable carboxylic acid and imidazole moieties. Chemical shift changes of the 2D resolvable C_α proton resonances were used to examine for any possible

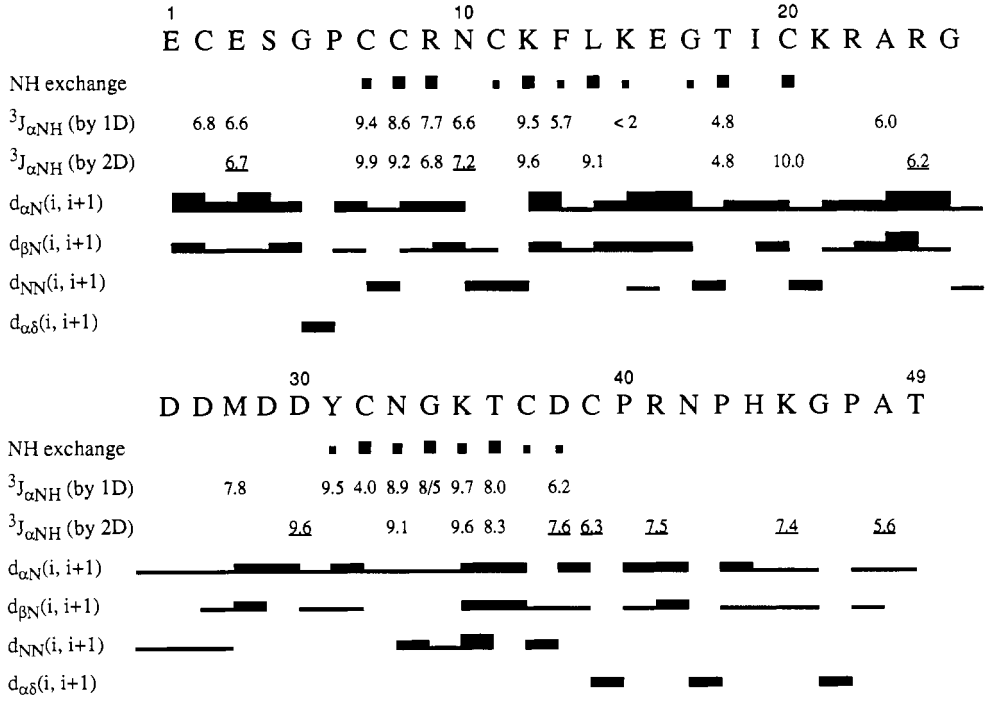

FIGURE 5: Summary of the observed, sequential NOEs and coupling constants used in the assignments. Sequential NOEs are indicated as lines below the sequence. Slowly exchanging amide protons are indicated by a filled square below the one-letter code of the corresponding amino acid residue. Larger squares denote more slowly exchanging amide protons. The coupling constants were obtained by either peak deconvolution of 1D spectra or by the method of Kim and Prestegard from 2D spectra. The latter were measured from DQF-COSY spectra of echistatin in D_2O and echistatin in 90% H_2O/10% D_2O (underlined).

Table I: Proton Resonance Assignments for Echistatin at pH 3.1 and 27 °C[a]

residue	NH	$C_\alpha H$	$C_\beta H$	$C_\gamma H$	others
Glu1		4.03	2.12, 2.12	2.42, 2.42	
Cys2	8.90	4.68	3.22, 3.14		
Glu3	8.67	4.28	2.08, 1.83	2.40, 2.40	
Ser4	8.46	4.80	3.75, 3.75		
Gly5	8.36	4.35, 4.00			
Pro6		4.53	2.63, 1.90	2.21, 2.12	δCH_2 3.92, 3.63
Cys7	8.82	5.02	3.97, 2.74		
Cys8	8.31	5.18	3.31, 2.36		
Arg9	8.76	4.50	1.74, 1.65	1.54, 1.54	δCH_2 3.32, 3.25; ϵNH 7.21
Asn10	9.79	4.38	2.96, 2.66		δNH_2 7.54, 6.85
Cys11	8.89	4.35	3.54, 3.40		
Lys12	7.61	4.38	1.76, 1.65	1.36, 1.36	δCH_2 1.65, 1.65; ϵCH_2 2.96, 2.96; ζNH_3^+ 7.50
Phe13	7.95	4.71	3.04, 2.63		2,6H 7.05; 3,4,5H 7.19
Leu14	8.92	4.37	1.80, 1.50	1.33	δCH_3 1.00, 0.88
Lys15	8.16	4.05	1.75, 1.75	1.45, 1.45	δCH_2 1.56, 1.56; ϵCH_2 3.00, 3.00; ζNH_3^+ 7.49
Glu16	8.92	3.86	1.90, 1.90	2.42, 2.38	
Gly17	8.64	4.33, 3.40			
Thr18	7.73	4.12	3.72	1.32	
Ile19	8.98	4.05	1.75	1.74, 1.01	γCH_3 0.80; δCH_3 0.92
Cys20	8.92	5.03	3.04, 2.93		
Lys21	7.68	4.39	1.73, 1.62	1.42, 1.28	δCH_2 1.66, 1.66; ϵCH_2 2.95, 2.95; ζNH_3^+ 7.50
Arg22	8.67	4.34	1.78, 1.60	1.54, 1.54	δCH_2 3.14, 3.14; ϵNH 7.28
Ala23	8.26	4.30	1.28		
Arg24	8.32	4.28	1.80, 1.74	1.64, 1.58	δCH_2 3.18, 3.18; ϵNH 7.18
Gly25	8.48	4.00, 3.82			
Asp26	8.38	4.71	2.87, 2.78		
Asp27	8.34	4.68	2.89, 2.82		
Met28	8.05	4.55	2.06, 1.87	2.59, 2.47	ϵCH_3 2.05
Asp29	8.25	4.64	2.56, 2.48		
Asp30	8.22	5.05	2.98, 2.42		
Tyr31	8.70	5.24	2.64, 2.56		2,6H 6.94; 3,5H 6.73
Cys32	9.52	4.78	3.96, 2.54		
Asn33	9.87	4.95	3.30, 2.82		δNH_2 7.68, 6.85
Gly34	8.30	4.22, 4.22			
Lys35	8.58	3.68	1.60, 1.37	1.08, 1.08	δCH_2 1.53, 1.47; ϵCH_2 2.87, 2.87; ζNH_3^+ 7.36
Thr36	7.55	4.63	4.37	1.18	
Cys37	8.97	4.72	2.75, 2.75		
Asp38	8.35	4.51	2.59, 2.52		
Cys39	8.79	5.53	2.93, 2.64		
Pro40		4.33	2.22, 1.82	2.08, 2.08	δCH_2 4.18, 3.68
Arg41	8.28	4.06	1.69, 1.69	1.64, 1.54	δCH_2 3.16, 3.16; ϵNH 7.22
Asn42	8.25	4.90	3.04, 2.82		δNH_2 7.91, 7.23
Pro43		4.49	2.22, 1.86	2.00, 1.78	δCH_2 3.86, 3.77
His44	8.59	4.62	3.32, 3.21		2H 8.63; 4H 7.35
Lys45	8.25	4.34	1.84, 1.74	1.44, 1.44	δCH_2 1.68, 1.68; ϵCH_2 3.02, 3.02; ζNH_3^+ 7.52
Gly46	8.24	4.12, 4.04			
Pro47		4.42	2.25, 1.95	2.02, 2.02	δCH_2 3.62, 3.62
Ala48	8.44	4.34	1.38		
Thr49	7.87	4.29	4.29	1.15	

[a] Assignments of degenerate chemical shifts for methylene protons are tentative.

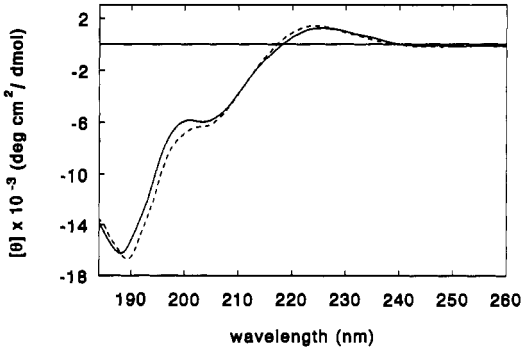

FIGURE 6: Far-UV CD spectra of echistatin dissolved in 5 mM sodium phosphate buffer, at pH values of 3.4 (solid line) and 7.3 (dashed line). The sample temperature was 26 °C.

change in secondary or tertiary structure. Overall, most of the C_α proton resonances shifted by 0.04 ppm or less, indicating little change in structure. The stretch of residues from Cys7 to Thr18 (except Leu14 which was overlapped and therefore not measured) showed good stability (Δ0.01 ppm or less) over the pH range. Shifts larger than 0.04 ppm were observed for the α protons of Glu1 (−0.06), Glu3 (−0.09), Gly5 (+0.05/−0.03) Ala23 (−0.19), Gly25 (−0.05/0.00), Asp29 (−0.08), Asp30 (−0.08), Tyr31 (+0.12), Thr36 (+0.06), Asn42 (−0.11), Pro43 (−0.06), His44 (−0.06), and Thr49 (−0.19). The Thr49 shift is easily explained by the expected ionization of the C-terminal carboxyl group. Glu1 and His44 show little change until the pH jump from 5.7 to 7.1, indicating that the observed changes are primarily due to the protonation states of the N-terminal ammonium and imidazole groups, respectively. The remaining shifts are more difficult to account for in a definitive way, but may be explained in part by the association of ionized groups. Out of 49 residues, echistatin contains 9 carboxyl groups and 11 basic sites. It would be reasonable to expect a change in the association equilibrium of flexible parts of the protein (see below) which contain some of these groups.

Perhaps the most remarkable shift from the titration study is the Ala23 C_α proton. Ala23 $C_\alpha H$ shifts from 4.30 ppm at pH 3.1 to 4.11 ppm at pH 7.1. The random-coil chemical shift for an alanine is 4.35 ppm (Wüthrich, 1986). The large shift

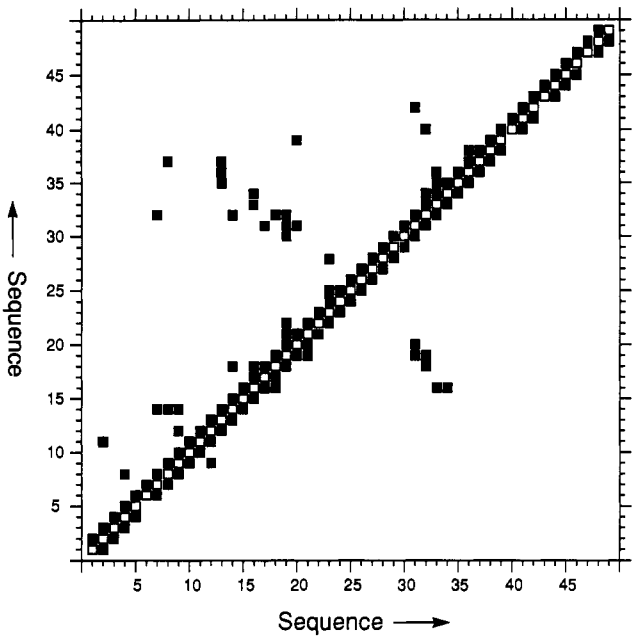

FIGURE 7: Diagonal plot of interresidue NOEs identified from NOESY spectra with mixing times up to 200 ms. Plotted below the diagonal are backbone to backbone NOEs. Connections above the diagonal represent all interresidue backbone and side-chain NOEs.

may be due to interactions of the neighboring Lys and Arg residues. It is noteworthy that the only effect of titration on the α-protons of the Arg-Gly-Asp binding moiety is an upfield shift of one of the Gly protons. Arg24, Asp26, and the other Gly25 $C_\alpha H$ do not shift more than 0.01 ppm.

Secondary Structure. NOEs, coupling constants, and amide hydrogen exchange rates (see Figures 7 and 5) suggest that the secondary structure of the protein is composed of a number of turns and loops. In particular, echistatin contains a type I β-turn between residues 5–8, a β-hairpin between residues 9–12, and a short, irregular, antiparallel β-sheet joining residues 18–20 and 30–32. The β-sheet can be seen in Figure 7 as points that are perpendicular to the diagonal. The Arg24-Gly25-Asp26 binding fragment is located in a loop of nine residues (21–29) connecting the two strands of the β-sheet. NOE evidence was found for assignment of two of the four disulfides in the protein. Schematic diagrams of the secondary structure of echistatin are presented in Figure 8.

Residues 5–8 form either a type I or type II′ turn on the basis of NOE and coupling constant data. There is a strong NH to NH NOE between residues 7 and 8, the $^3J_{C\alpha H\text{-}NH}$ coupling constant for residue 7 is >9 Hz, and the NH of Cys8 has a very slow rate of exchange with solvent. Only a very weak NOE is observed between Pro6 $C_\alpha H$ and Cys8 NH. The two types of turns can normally be distinguished on the basis of an NH to NH NOE between residues at the second and third positions of a four-residue reverse turn. Although the second position residue in this case does not have an NH since it is Pro6, the C_δ protons of the proline can be used as suitable reporter groups. A medium-strength NOE is indeed observed between the 3.92-ppm $C_\delta H$ of Pro6 and Cys7 NH, signifying that the turn is a type I. The ϕ angle of proline is limited to approximately −60° (Creighton, 1984a), and the ϕ_2 angle expected for a type II′ turn is +60°, lending further support for the turn being type I.

Residues 10 and 11 of the β-hairpin form either a type I or I′ β-turn according to the NOE pattern and hydrogen exchange information (Wüthrich et al., 1984). For a type I β-turn, the $^3J_{C\alpha H\text{-}NH}$ coupling constants for residues 10 and 11 are expected to be 4 and 9 Hz, respectively, whereas for a type I′ β-turn the coupling constants are expected to be 7 and 5 Hz, respectively. The $^3J_{C\alpha H\text{-}NH}$ coupling for residue 10 is 6.6 Hz while the value for residue 11 has not yet been determined. A rather weak correlation in the DQF-COSY spectrum from the NH proton of residue 11 to its C_α proton suggests that $^3J_{C\alpha H\text{-}NH}$ is more in line with being 5 rather than 9 Hz. Thus, the data suggest that the turn between residues 9–12 is a type I β-turn. NOEs expected between two strands of a β-sheet are observed primarily between residues in 8–9 and 12–14, as shown in Figure 8. The $^3J_{C\alpha H\text{-}NH}$ couplings for residues 8, 12, and 14 fall in the 8–10-Hz range, consistent with a β-sheet structure; residue 9 is approximately 7.5 Hz and residue 13 is 5.7 Hz. It appears that the central portion of the sheet is slightly distorted as evidenced by the relatively small coupling constant of residue 13 and the lack of NH to $C_\alpha H$ NOE between residues 9 and 13. However, the slowly exchanging amides of residues 9 and 12 are consistent with hydrogen bonding between the strands of an antiparallel sheet.

An irregular, antiparallel β-sheet is located between residues 30–32 and 18–20. Most of the expected NOEs between the two chains are observed, as indicated by arrows in Figure 8. The $^3J_{C\alpha H\text{-}NH}$ coupling constants for residues 19 and 31 are large and consistent with β structure, but residues 18 and 32 have $^3J_{C\alpha H\text{-}NH}$ couplings of 4.8 and 4.0 Hz, respectively. In order to maintain the NOE between residues 18 and 32 and have torsion angles consistent with the small $^3J_{C\alpha H\text{-}NH}$ coupling constants, it appears that the hydrogen bond between residues 18 and 32 cannot exist. The hydrogen–deuterium exchange rate of the amide protons of residue 20 is very slow, consistent with hydrogen bonding between residues 20 and 30.

The NMR data do not suggest any α-helix in the protein in agreement with the CD results (see above). Not consistent with the CD data, however, are insufficient amounts of *regular* β-sheet and β-turns from the NMR data to account for the percentages of secondary structure estimated from the CD data. The discrepancy presumably results from the nonstandard secondary structures which make up echistatin. First, 16 of 29 measured $^3J_{C\alpha H\text{-}NH}$ couplings shown in Figure 5 are larger than ~7 Hz. Although not unique, couplings of this magnitude are typically found in β-sheets where ϕ angles are usually −119° or −139° (Wüthrich, 1986). This is suggestive of a number of strands of extended residues which may or may not be paired in a β-sheet, but with amide planes oriented within the strand as if they were in a β-sheet. The type I and β-hairpin turns discussed above are the only regular turns identified to date by NMR in the secondary structure of echistatin. A number of other turns must also be present since echistatin contains 4-disulfides which presumably stitch the protein together into a convoluted structure.

Echistatin contains 8 Cys residues at positions 2, 7, 8, 11, 20, 32, 37, and 39. Disulfide bonds between Cys2–Cys11 and Cys20–Cys39 are suggested from the NMR data. In the 200-ms mixing time NOESY experiment there are NOEs between the $C_\alpha H$ of Cys2 and the C_β protons of Cys11, between the $C_\alpha H$ of Cys39 and the C_β protons of Cys20, and between the $C_\alpha H$ of Cys20 and the C_β protons of Cys39. The case for the 2 remaining disulfides is less clear. NOEs are observed between the NH proton of Cys7 and one of the C_β protons of Cys32, and between the C_β protons of Cys8 and Cys37. The close proximity of residues 7 and 8 raises the possibility that the 7–32 and 8–37 NOEs could result from disulfide pairings of 7–32/8–37 or from 8–32/7–37. The protein can be folded in a similar manner with either pairing as shown schematically in Figure 8B. Recently, Calvete and co-workers (Calvete et al., 1991) published the disulfide pairing

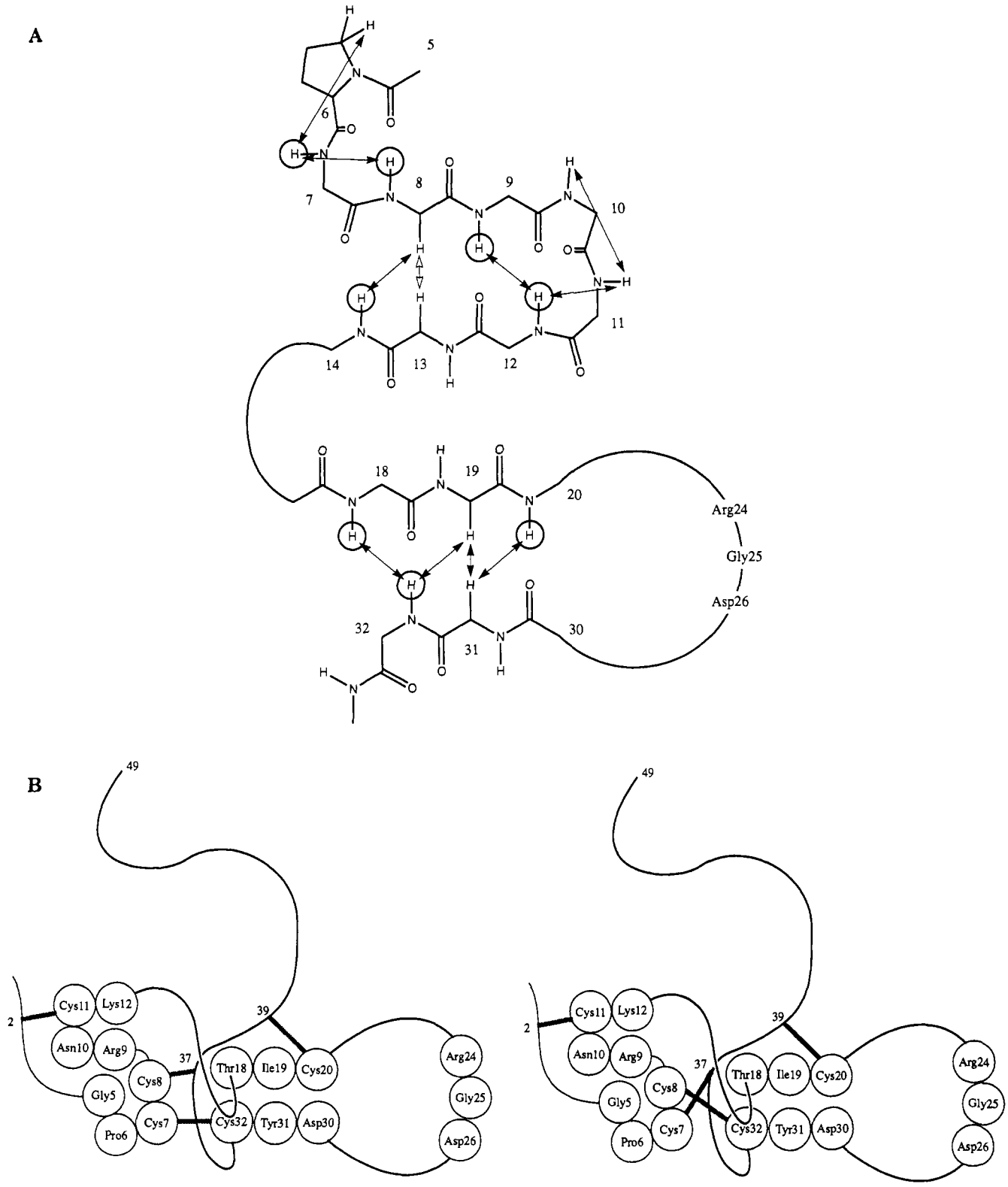

FIGURE 8: (A) Schematic representation of the secondary structure of echistatin. The double arrows represent the observed, nonsequential NOEs. The NOE between $C_\alpha H$ of residue 8 and $C_\alpha H$ of residue 13 is represented with a hollow arrow since it was only observed in the 450-ms mixing time NOESY experiment. Slowly exchanging NHs are indicated with circles. These data, together with vicinal $^3J_{C_\alpha H\text{-}NH}$ coupling constants, suggest that the β-turns and a short antiparallel β-sheet form the core of the protein; the Arg-Gly-Asp sequence is on a loop connecting the two strands of the β-sheet formed between residues 18–20 and 30–32. (B) Schematic representation of the global fold of echistatin for two possible disulfide pairings. On the left, residues 2–11, 20–39, 7–32, and 8–37 are paired. On the right, residues 2–11, 20–39, 8–32, and 7–37 are paired. Both pairings are consistent with the NMR data.

of albolabrin, a snake venom protein which is larger than echistatin, but which has a moderate degree of homology between its C-terminal end and echistatin (Figure 9). With 7 of the 8 cysteines of echistatin in alignment with albolabrin, it is conceivable that 3 of the disulfides have common pairings (Calvete et al., 1991). As shown in Figure 9, the NMR assignment of the 20–39 disulfide is in agreement with the albolabrin structure while the 2–11 pairing is not. Thus, structure analogy is not of use in this particular case for differentiating the 7–32/8–37 pairing from the 8–32/7–37

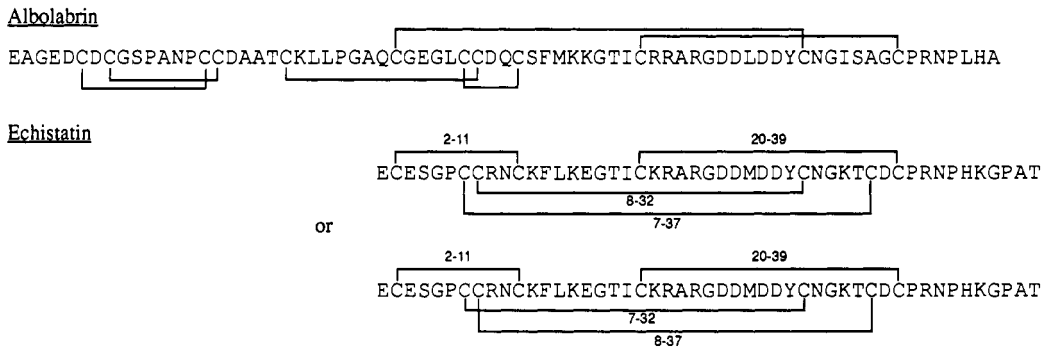

FIGURE 9: Sequences and disulfide pairings for albolabrin (Calvete et al., 1991) and echistatin. Both sets of disulfide pairings for echistatin are consistent with the NMR data.

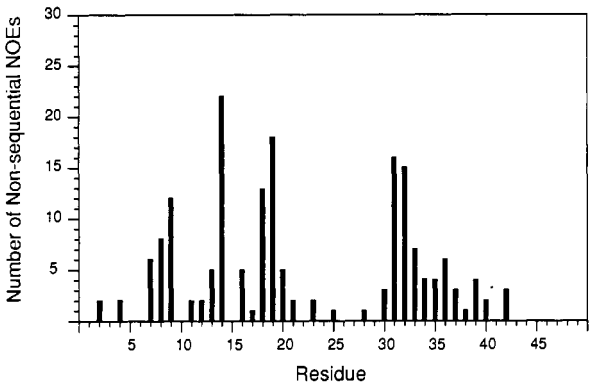

FIGURE 10: Plot of the total number of nonsequential, interresidue NOEs identified for each residue. Structured regions of the protein are characterized by large numbers of NOEs. The 9-residue loop containing the Arg-Gly-Asp moiety is found at residues 21–29 and exhibits few nonsequential NOEs.

pairing. We are attempting to distinguish between the disulfide pairs by looking for energetic differences in energy-minimized structures calculated for each pair.

The principal, but not necessarily exclusive, Gp IIb/IIIa binding site of echistatin and related snake venom proteins is believed to be the sequence Arg-Gly-Asp (Gould et al., 1990; Savage et al., 1990). In echistatin, this binding fragment is located in the middle of a loop of 9 residues (21–29) connecting two strands of a distorted β-sheet. In trying to determine the type of turn that might be adopted in this loop, it became apparent that many nonsequential, interresidue NOEs which are typical of secondary structures are absent from this region. Since interresidue NOEs are highly dependent on a specific conformation, any averaging of NOEs due to conformational mobility is expected to reduce the intensity of the observed NOEs. If the averaging is extensive, i.e., from many conformations, then the intensities of the averaged NOEs may diminish to the point of not being observed. This is dramatically illustrated in Figure 10 for the conformationally mobile regions of echistatin. Numerous interresidue NOEs are observed for the structured parts of the protein while very few interresidue NOEs are observed for the termini and the flexible loop containing the Arg-Gly-Asp sequence. Consistent with the concept of a flexible loop are the observed $^3J_{C\alpha H\text{-}NH}$ coupling constants for Ala23 and Arg24 (see Figure 5). The observed values of 6.0 and 6.2 Hz agree well with those expected if the backbone in this region is undergoing conformational changes on the NMR time scale. The fast solvent exchange rate for the amides in the loop region (see Figure 5) is further evidence for flexibility.

The consequence of echistatin's Arg-Gly-Asp binding fragment being conformationally mobile is that the conformation of the bound state (assuming that echistatin binds as a single conformation) cannot be directly deduced from the solution conformation. The flexibility of the binding region may, however, be a crucial factor in Gp IIb/IIIa inhibition by echistatin and by other Arg-Gly-Asp-containing peptides which are conformationally mobile (Bogusky et al., 1992). A lock-and-key model for ligand–receptor binding, where the key has a rigid conformation, is probably inappropriate for ligands that have multiple interaction points as in the case of Arg-Gly-Asp interacting with Gp IIb/IIIa. A "zipper" model has been proposed for the binding of flexible ligands to macromolecules as a means for explaining the kinetics of multipoint binding interactions (Burgen et al., 1975).

Conclusions

The proton NMR spectrum of echistatin is assigned, and the results were used to determine secondary structure elements of the protein. A type I β-turn exists at residues 5–8, a β-hairpin is found at residues 8–13, and an irregular β-sheet is found between residues 18–20 and residues 30–32. Additional turns and extended chains are inferred from the results of CD spectrophotometry. NMR evidence is found for disulfide linkages from residues 2 to 11 and 20 to 39. The spatial proximity of the remaining 4 Cys groups prevented elucidation of their disulfide pairing. Mobility is observed in the C- and N-terminal regions of the molecule. The protein contains a tripeptide sequence, Arg-Gly-Asp, which is largely responsible for echistatin's affinity for the Gp IIb/IIIa receptor complex. This tripeptide recognition unit is found in a flexible loop connecting the two strands of the β-sheet. The flexible nature of the binding site is probably an important feature of echistatin and other peptides and proteins containing the Arg-Gly-Asp recognition unit.

Added in Proof

During the review of this paper, Saudek and co-workers (Saudek et al., 1991) independently published calculations on the three-dimensional structure of echistatin.

Acknowledgments

We thank Dr. Chuan Wang (Rutgers University) and Drs. Michael Bogusky, Robert Gould, and Adel Naylor (Merck Sharp & Dohme Research Labs) for many helpful discussions. We thank Dr. Paul Anderson (Merck Sharp & Dohme Research Labs) for his support and encouragement.

Registry No. Echistatin, 129038-42-2.

References

Bax, A., & Freeman, R. (1981) *J. Magn. Reson. 44*, 542–561.
Bax, A., & Davis, D. (1985) *J. Magn. Reson. 65*, 355–360.
Billeter, M., Braun, W., & Wüthrich, K. (1982) *J. Mol. Biol. 155*, 321–346.
Bogusky, M. J., Naylor, A. M., Pitzenberger, S. M., Nutt, R. F., Brady, S. F., Colton, C. D., Sisko, J. T., Anderson, P.

S., & Veber, D. F. (1992) *Int. J. Pept. Protein Res.* (in press).
Braunsweiler, L., & Ernst, R. R. (1983) *J. Magn. Reson. 53*, 521–528.
Bundi, A., & Wüthrich, K. (1979) *Biopolymers 18*, 285–297.
Burgen, A. S. V., Roberts, G. C. K., & Feeney, J. (1975) *Nature 253*, 753–755.
Bush, L. R., Holahan, M. A., Kanovsky, S. M., Mellott, M. J., Garsky, V. M., & Gould, R. J. (1989) *Circulation 80*, II-23.
Calvete, J. J., Schäfer, W., Soszka, T., Lu, W., Cook, J. J., Jameson, B. A., & Niewiarowski, S. (1991) *Biochemistry 30*, 5225–5229.
Cantor, C. R., & Schimmel, P. R. (1980) *Biophysical Chemistry*, Part II, W. H. Freeman and Co., San Francisco.
Coller, B. S., Folts, J. D., Smith, S. R., Scudder, L. E., & Jordan, R. (1989) *Circulation 80*, 1766–1774.
Creighton, T. E. (1984a) *Proteins, Structures and Molecular Principles*, W. H. Freeman and Co., New York.
Creighton, T. E. (1984b) *Methods Enzymol. 107*, 305–329.
Dennis, M. S., Henzel, W. J., Pitti, R. M., Lipari, M. T., Napier, M. A., Deisher, T. A., Bunting, S., & Lazarus, R. A. (1990) *Proc. Natl. Acad. Sci. U.S.A. 87*, 2471–2475.
Eich, G., Bodenhausen, G., & Ernst, R. R. (1982) *J. Am. Chem. Soc. 104*, 3731–3732.
Gan, Z.-R., Gould, R. J., Jacobs, J. W., Friedman, P. A., & Polokoff, M. A. (1988) *J. Biol. Chem. 263*, 19827–19832.
Garsky, V. M., Lumma, P. K., Freidinger, R. M., Pitzenberger, S. M., Randall, W. C., Veber, D. F., Gould, R. J., & Friedman, P. A. (1989) *Proc. Natl. Acad. Sci. U.S.A. 86*, 4022–4026.
Gartner, T. K., & Bennett, J. S. (1985) *J. Biol. Chem. 260*, 11891–11894.
Genest, M., Marion, D., Caille, A., & Ptak, M. (1989) *Colloq. INSERM, Forum Pept., 2nd, 1988 174*, 415–418.
Ginsberg, M. H., Loftus, J. C., & Plow, E. F. (1988) *Thromb. Haemostasis 59*, 1–6.
Glasoe, P. K., & Long, F. A. (1960) *J. Phys. Chem. 64*, 188–190.
Gold, H. K., Coller, B. S., Yasuda, T., Saito, T., Fallon, J. T., Guerrero, J. L., Leinbach, R. C., Ziskind, A. A., & Collen, D. (1988) *Circulation 77*, 670–677.
Gould, R. J., Polokoff, M. A., Friedman, P. A., Huang, T.-F., Holt, J. C., Cook, J. J., & Niewiarowski, S. (1990) *Proc. Soc. Exp. Biol. Med. 195*, 168–171.
Huang, T.-F., Holt, J. C., Lukasiewicz, H., & Niewiarowski, S. (1987) *J. Biol. Chem. 262*, 16157–16163.
Hynes, R. O. (1987) *Cell 48*, 549–554.
Kay, L. E., Jones, P.-J., & Prestegard, J. H. (1987) *J. Magn. Reson. 72*, 392–396.
Kim, Y., & Prestegard, J. H. (1989) *J. Magn. Reson. 84*, 9–13.
Kumar, A., Ernst, R. R., & Wüthrich, K. (1980) *Biochem. Biophys. Res. Commun. 95*, 1–6.
Levitt, M. H., Freeman, R., & Frenkiel, T. (1982) *J. Magn. Reson. 47*, 328–330.
Manavalan, P., & Johnson, W. C., Jr. (1987) *Anal. Biochem. 167*, 76–85.
Marion, D., & Wüthrich, K. (1983) *Biochem. Biophys. Res. Commun. 113*, 967–974.
McGoff, M. A., Allen, B. T., Sicard, G. A., Anderson, C. B., & Santoro, S. A. (1989) *Circulation 80*, II-23.
Mickos, H., Bahr, J., & Lüning, B. (1990) *Acta Chem. Scand. 44*, 161–164.
Mueller, L., & Ernst, R. R. (1979) *Mol. Phys. 38*, 963–992.
Nagayama, K., Kumar, A., Wüthrich, K., & Ernst, R. R. (1980) *J. Magn. Reson. 40*, 321–334.
Nègre, E., Marion, D., Roche, A. C., Monsigny, M., & Mayer, R. (1989) *Colloq. INSERM, Forum Pept., 2nd, 1988 174*, 575–578.
Otting, G., & Wüthrich, K. (1987) *J. Magn. Reson. 75*, 546–549.
Otting, G., Widmer, H., Wagner, G., & Wüthrich, K. (1986) *J. Magn. Reson. 66*, 187–193.
Phillips, D. R., Charo, I. F., Parise, L. V., & Fitzgerald, L. A. (1988) *Blood 71*, 831–843.
Pierschbacher, M. D., & Ruoslahti, E. (1984) *Nature 309*, 30–33.
Plow, E. F., Ginsberg, M. H., & Marguerie, G. A. (1986) in *Biochemistry of Platelets* (Phillips, D. R., & Shuman, M. A., Ed.) pp 225–256, Academic Press, Orlando.
Rance, M., Sorensen, O. W., Bodenhausen, G., Wagner, G., Ernst, R. R., & Wüthrich, K. (1983) *Biochem. Biophys. Res. Commun. 117*, 479–485.
Redfield, A. G., & Kunz, S. D. (1975) *J. Magn. Reson. 19*, 250–254.
Reed, J., Hull, W. E., von der Lieth, C.-W., Kübler, D., Suhai, S., & Kinzel, V. (1988) *Eur. J. Biochem. 178*, 141–154.
Ruoslahti, E., & Pierschbacher, M. D. (1986) *Cell 44*, 517–518.
Ruoslahti, E., & Pierschbacher, M. D. (1987) *Science 238*, 491–497.
Saudek, V., Atkinson, R. A., & Pelton, J. T. (1991) *Biochemistry 30*, 7369–7372.
Savage, B., Marzec, U. M., Chao, B. H., Harker, L. A., Maraganore, J. M., & Ruggeri, Z. M. (1990) *J. Biol. Chem. 265*, 11766–11772.
Shaka, A. J., & Freeman, R. (1983) *J. Magn. Reson. 51*, 169–173.
Shebuski, R. J., Ramjit, D. R., Bencen, G. H., & Polokoff, M. A. (1989a) *J. Biol. Chem. 264*, 21550–21556.
Shebuski, R. J., Berry, D. E., Bennett, D. B., Romoff, T., Storer, B. L., Ali, F., & Samanen, J. (1989b) *Thromb. Haemostasis 61*, 183–188.
States, D. J., Haberkorn, R. A., & Ruben, D. J. (1982) *J. Magn. Reson. 48*, 286–292.
Steiner, B., Cousot, D., Trzeciak, A., Gillessen, D., & Hadváry, P. (1989) *J. Biol. Chem. 264*, 13102–13108.
Wagner, G., & Wüthrich, K. (1982) *J. Mol. Biol. 155*, 347–366.
Wider, G., Lee, K. H., & Wüthrich, K. (1982) *J. Mol. Biol. 155*, 367–388.
Wüthrich, K. (1986) *NMR of Proteins and Nucleic Acids*, Wiley-Interscience Publication, New York.
Wüthrich, K., Billeter, M., & Braun, W. (1984) *J. Mol. Biol. 180*, 715–740.
Yasuda, T., Gold, H. K., Fallon, J. T., Leinbach, R. C., Guerrero, J. L., Scudder, L. E., Kanke, M., Shealy, D., Ross, M. J., Collen, D., & Coller, B. S. (1988) *J. Clin. Invest. 81*, 1284–1291.